

Probing the Near-Field of Second-Harmonic Light around Plasmonic Nanoantennas

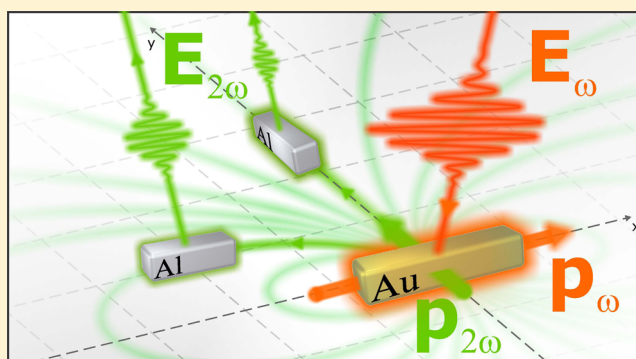
Bernd Metzger,*¹ Mario Hentschel, and Harald Giessen

¹ Physics Institute and Research Center SCoPE, University of Stuttgart, Pfaffenwaldring 57, 70569 Stuttgart, Germany

Supporting Information

ABSTRACT: We introduce a new concept that enables subwavelength polarization-resolved probing of the second-harmonic near-field distribution of plasmonic nanostructures. As a local sensor, this method utilizes aluminum nanoantennas, which are resonant to the second-harmonic wavelength and which allow to efficiently scatter the local second-harmonic light to the far-field. We place these sensors into the second-harmonic near-field generated by plasmonic nanostructures and carefully vary their position and orientation. Observing the second-harmonic light resonantly scattered by the aluminum nanoantennas provides polarization-resolved information about the local second-harmonic near-field distribution. We then investigate the polarization-resolved second-harmonic near-field of inversion symmetric gold dipole nanoantennas. Interestingly, we find strong evidence that the second-harmonic dipole is predominantly oriented perpendicular to the gold nanoantenna long axis, although the excitation laser is polarized parallel to the nanoantennas. We believe that our investigations will help to disentangle the highly debated origin of the second-harmonic response of inversion symmetric plasmonic structures. Furthermore, we believe that our new method, which enables the measurement of local nonlinear electric fields, will find widespread implementation and applications in nonlinear near-field optical microscopy.

KEYWORDS: Near-field optical microscopy, nonlinear plasmonics, nano optics, second-harmonic generation



Subdiffraction limited super-resolution microscopies have revolutionized the field of optical microscopy and are providing scientists with the ability to observe and manipulate matter at length scales much smaller than the wavelength of light. Among others, stimulated emission depletion (STED) microscopy¹ and photoactivated localization microscopy (PALM),² for example, enable imaging of biological samples down to nanometer length scales. Furthermore, time-resolved two photon photoemission electron microscopy enables femtosecond temporal resolution with simultaneous nanometer spatial resolution.³ Scattering near-field optical microscopy (SNOM), which uses the strongly confined evanescent field of a nanoscale tip to image subwavelength features on a surface, even allows one to measure spectrally resolved molecular response functions.^{4,5} Additionally, because of its high sensitivity to localized electromagnetic fields it has been widely used to study the electric near-field distribution of plasmonic nanostructures,^{6,7} which are of great importance, for example, for refractive index sensing based on plasmonic antennas,^{8–10} plasmon-enhanced vibrational spectroscopy,^{11,12} enhancement of nonlinear optical effects,^{13–15} and coupling of single quantum emitters to plasmonic cavities.¹⁶ Hence, there has been great interest in understanding the linear optical near-field of plasmonic nanostructures using SNOM, which has been realized even in a polarization-resolved fashion.¹⁷

However, in contrast to the linear optical fields, the nonlinear optical near-fields generated by plasmonic nanostructures barely have been studied in a spatially resolved fashion on a subwavelength scale,¹⁸ although there have been numerous far-field spectroscopic investigations of the nonlinear optical response of plasmonic nanostructures.^{13,19–35} Information about the spatial distribution of the nonlinear near-fields of plasmonic nanostructures is key to unravel the microscopic mechanism that leads to second-harmonic (SH) generation from inversion symmetric plasmonic structures, which still is under debate. Furthermore, we can provide a design recipe for how different plasmonic elements or other nanoscale systems can be efficiently coupled to the nonlinear near-field of plasmonic nanostructures.

In this Letter, we propose and realize a new method that enables probing the local nonlinear SH field of plasmonic nanostructures in a polarization-resolved subwavelength fashion. We utilize SH resonant aluminum nanoantennas as local sensors to probe the SH near-field of gold dipole nanoantennas.^{36,37} As a consequence of their SH resonant behavior, the aluminum nanoantennas scatter the local SH field

Received: December 20, 2016

Revised: February 7, 2017

Published: February 9, 2017

much stronger when compared to the SH signal that is directly emitted from the gold nanoantennas. This circumstance warrants an efficient far-field background suppression commonly required in subdiffraction limited microscopies.^{38,39}

In contrast to most of the above-mentioned subdiffraction limited microscopies, the experiments carried out here are ensemble measurements of plasmonic nanoantenna arrays. However, our method still allows gathering subwavelength spatially resolved information about the localized nonlinear near-fields, similar to previous studies of the linear optical near-field of three-dimensional plasmonic structures.⁴⁰

The physical mechanism behind our SH near-field mapping technique is sketched in Figure 1a. First, in the gold dipole

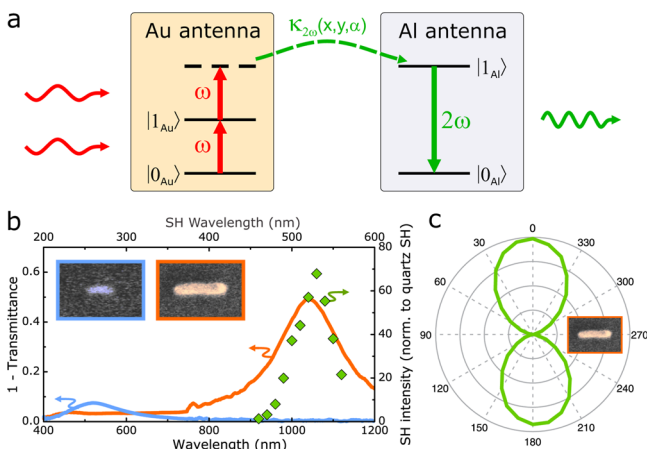


Figure 1. (a) Sketch of the physical mechanism of SH near-field probing of gold nanoantennas. (b) Measured $1 - \text{Transmittance}$ spectra of a gold (orange) and an aluminum (blue) nanoantenna array as well as measured SH spectroscopy (green, diamonds) of the gold nanoantenna array plotted over the fundamental excitation wavelength. The top axis shows the corresponding SH wavelength. The insets show SEM images of a single gold and aluminum nanoantenna element, which have a length of about 200 and 100 nm, respectively. Their nominal width and height are both 50 nm. (c) Measured polarization-resolved SH intensity of the gold nanoantenna array at the peak of the SH response at 1060 nm. We find the polarization of the emitted SH signals almost perfectly oriented perpendicular to the gold nanoantennas.

nanoantennas, which are designed to be resonant to our laser excitation frequency ω , two photons resonantly create a SH polarization in an off-resonant virtual state. From this virtual state in the gold nanoantennas, the SH polarization either can decay into absorption or it can be directly radiated to the far-field with the latter having a quite weak efficiency because the off-resonant virtual state does not efficiently couple to the far-field. However, when introducing aluminum nanoantennas close to the gold nanoantennas, which are resonant to the virtual state of the gold nanoantennas, and hence to the SH wavelength, SH energy can be transferred to the aluminum antennas before direct scattering or absorption occurs. The efficiency of this process, and hence the coupling rate $\kappa_{2\omega}$ between the gold and the aluminum nanoantennas, strongly depends on the spatial coordinates x and y of the aluminum nanoantenna with respect to the gold antenna, as well as on the orientation angle α of the aluminum antenna. Subsequently, from the excited state in the aluminum antennas SH energy can efficiently be radiated to the far-field.

The plasmonic nanoantenna arrays are fabricated by electron beam lithography (EBL) on fused silica substrates. In order to fabricate hybrid gold–aluminum plasmonic nanostructure arrays, we utilize a two-step EBL process. First, we fabricate a large set of identical gold dipole nanoantenna arrays. These nanostructure arrays have a lattice constant of 500 nm and an area of $100 \times 100 \mu\text{m}^2$, see Figure 1 for the corresponding geometrical parameters of the antenna elements. Second, for the subsequent experiments to probe the local SH field of the gold dipole nanoantennas we position in a second EBL process aluminum nanoantennas next to the already existing gold nanoantennas, and carefully vary their position and orientation.

In advance to the measurements of the local SH near-field distribution of gold dipole nanoantennas, we characterized the far-field linear and SH response of the individual systems, that is, the response of a bare gold and a bare aluminum nanoantenna array, respectively.

We measured transmittance spectra T using a broadband white light source polarized along the long axis of the nanoantennas. The corresponding measured $1 - T$ spectra of a gold and an aluminum nanoantenna array are shown in Figure 1b. We find a longitudinal plasmon resonance at about 1040 and 520 nm of the gold and the aluminum nanoantenna array, respectively. Hence, as desired the linear optical response of the aluminum nanoantennas is resonant to the SH response of the gold nanoantennas.

We also performed SH spectroscopy of the individual nanoantenna arrays. Therefore, we focused sub-30 fs laser pulses tunable from 920 to 1120 nm under normal incidence on the nanoantenna arrays using an achromatic lens with a focal lens of 75 mm, which leads to a focus spot diameter of about $50 \mu\text{m}$ on the nanoantenna arrays. As in the transmittance measurements the polarization of the incident laser light was oriented along the nanoantenna axes. The generated SH signals radiated in forward direction were collected using a fused silica lens, then filtered to remove the fundamental laser light, analyzed by a polarizer, and measured using a Peltier-cooled charge-coupled device camera attached to a spectrometer. Finally, to obtain a scalar value describing the SH intensity, the measured SH spectra were integrated, and normalized to a SH signal generated on a quartz substrate in reflection.^{41,42}

In Figure 1b, the normalized SH intensities from a gold nanoantenna array together with its transmittance spectrum are shown. As in earlier work on third-harmonic (TH) generation we find the peak of the SH intensity slightly red-shifted with respect to the linear optical far-field spectrum.⁴³ Noteworthy, the measured SH signals investigated here are found to be about an order of magnitude weaker when compared to measured TH signals from the same gold nanoantenna arrays, which we predominantly attribute to the isotropy of the poly crystalline metals as well as to the inversion symmetry of the overall antenna geometry, which we further discuss below. Most surprisingly, in contrast to the radiated TH signals from gold nanoantenna arrays, which are highly polarized along the nanoantenna long axes (not shown), we find the polarization of the SH intensity to be strongly oriented perpendicular to the gold nanoantennas with a ratio of the two orthogonal polarization components of about 250 to 1. To quantitatively measure this polarization behavior we analyzed the SH signals using the aforementioned polarizer and rotated it in 10° steps over 360° and simultaneously recorded the transmitted SH intensity. A corresponding polar SH intensity distribution is shown in Figure 1c.

We also performed SH spectroscopy of a bare aluminum nanoantenna array. We find the SH response at least 3 orders of magnitude weaker as compared to the SH response of the resonant gold nanoantenna array, see Figure S1 in the Supporting Information. The main reason for the very weak SH response of the aluminum nanoantennas is that they are not resonant to the excitation laser wavelength. Hence, in the following it is reasonable to neglect the weak SH signals generated by far-field excitation in the bare aluminum nanoantennas. Noteworthy, there is still the possibility that the SH response of the aluminum nanoantennas contributes to the overall SH response, because the near-field of the gold nanoantennas at the fundamental wavelength also enhances the SH response of the aluminum antennas. However, simulated near-field distributions, which are shown in the Supporting Information Figure S2, show that the fundamental near-field on the surface of the gold nanoantennas is much stronger when compared to the fundamental field at the position of the aluminum nanoantennas. This underlines that the corresponding process is most likely not a relevant mechanism in our experiments. Furthermore, our experimental findings cannot be described when assuming that the near-field of the gold nanoantennas is driving the SH response of the aluminum nanoantennas, which we will explain further below.

It is interesting and unexpected that we observe a SH signal at all. In dipole approximation, SH generation of inversion symmetric structures, such as the gold dipole nanoantennas, is forbidden by symmetry.^{44–46} To date, the origin of the SH response of inversion symmetric plasmonic structures still is under debate. Possible mechanisms for the origin of the SH response are local symmetry-breaking defects on the surface of the antennas.⁴⁷ Furthermore, the substrate breaks the symmetry normal to the propagation direction and hence symmetry-allowed tensor elements could contribute to a nonvanishing second-order response. Finally, also higher order magnetic dipole or electric quadrupole contributions might play an important role for SH generation of inversion symmetric plasmonic structures.⁴⁸

In order to shine some light on these unanswered questions and to demonstrate our new method, in the following we are going to probe the local SH near-field of inversion symmetric gold dipole nanoantennas using the aluminum nanoantennas as local SH near-field sensors.

In the first SH near-field experiments, we are going to probe the x -component of the local SH near-field, that is, the field-component along the gold nanoantenna long axis. Hence, we align aluminum nanoantennas in a parallel fashion with respect to the gold nanoantennas. In Figure 2a, we illustrate the corresponding experiment; Figure 2b shows corresponding scanning electron micrographs (SEM) of a fabricated sample.

In the experiment, we again focus sub-30 fs laser pulses polarized along the gold nanoantenna long axis on the hybrid gold–aluminum nanoantenna arrays, however, this time we keep the excitation wavelength fixed at 1060 nm, which is close to the peak of the SH response of the gold nanoantennas. As mentioned before, because only the gold nanoantennas are resonant to the laser wavelength, the incident laser light almost exclusively interacts with the gold nanoantennas and not with the aluminum nanoantennas. Hence, solely at the gold nanoantennas SH radiation is generated. Subsequently, SH energy is transferred from the gold nanoantennas via the SH near-field to the aluminum nanoantennas and from there efficiently scattered to the far-field. Notably, the SH signals

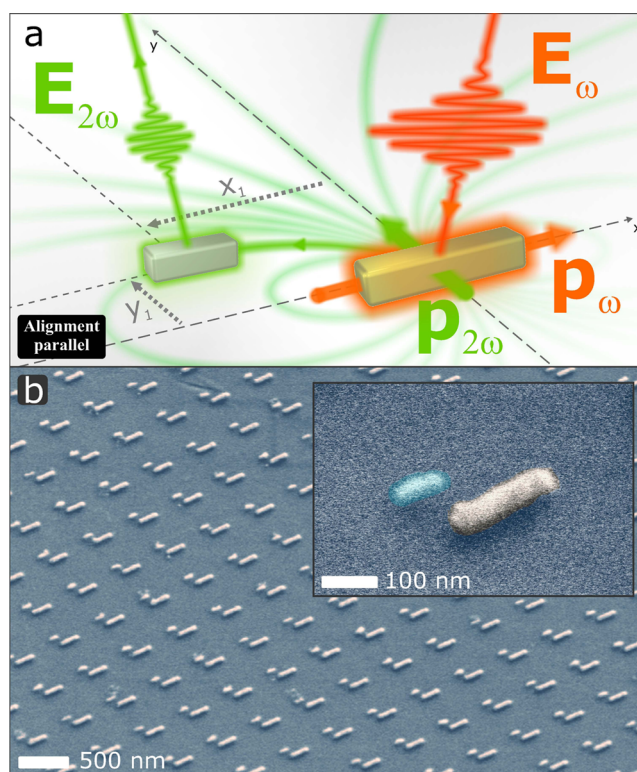


Figure 2. (a) Graphical illustration of the experiment: Probing the x -component of the local SH near-field of gold nanoantennas. (b) Colored-tilted SEMs of a corresponding sample.

radiated from the aluminum antennas are polarized parallel to the aluminum nanoantenna long axes due to their SH resonant behavior. The efficiency of the SH energy transfer from the gold to the aluminum antennas strongly depends on the precise position and orientation of the aluminum nanoantennas. In particular, SH energy can only be transferred when the aluminum nanoantenna axis is oriented in a parallel fashion with respect to a field component of the SH near-field of the gold nanoantennas (see sketch in Figure 2a).

In the following, we shift the aluminum nanoantennas in small steps of nominally 20 nm along the gold nanoantennas, that is, from a centered position with an aluminum antenna offset $x_1 \approx 0$ nm to $x_1 \approx 190$ nm and with a constant offset in the y -direction y_1 of about 125 nm, see Figure 2 and the SEM images in Figure 3a. This shift does almost not influence the plasmon resonance and the field-enhancement of the gold nanoantennas, which can be inferred from electrodynamic near-field simulations at the fundamental wavelength and measured linear optical spectra of the corresponding nanoantenna arrays, which are shown in the Supporting Information in the Figures S2 and S3, respectively. Hence, the SH generation in the gold nanoantennas is expected to be equally efficient for the different nanoantenna arrays. For every nanoantenna array, we measure the x -polarized SH intensity and normalize it to the x -polarized SH signal radiated from a bare gold nanoantenna array without aluminum nanoantennas. The corresponding measured SH intensities are plotted in Figure 3a over the aluminum antenna offset x_1 , which has been extracted from SEM images. We find a peak in the radiated x -polarized SH intensity at $x_1 \approx 80$ nm. For $x_1 = 0$ nm, as well as for large aluminum antenna offsets x_1 the SH intensity approaches the weak x -polarized SH intensity radiated from the bare gold nanoantenna array.

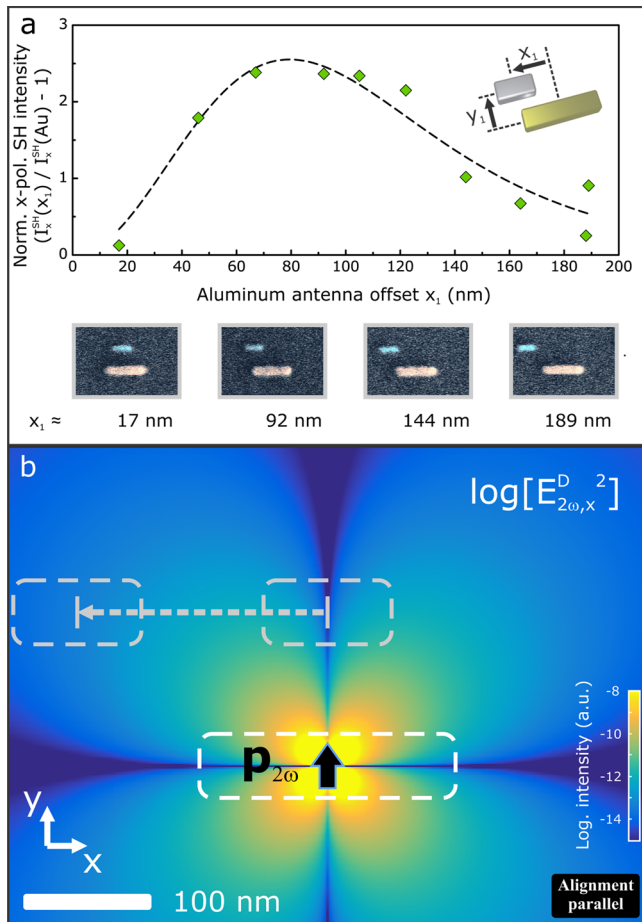


Figure 3. (a) Measured x -polarized SH intensity as a function of the aluminum antenna offset x_1 . The black dashed line corresponds to a fitted dipolar intensity distribution using eq 2. The insets below show exemplary colored SEM images. (b) Dipole field intensity distribution of the x -component of a static electric SH dipole $\mathbf{p}_{2\omega}$ oriented along the y -direction. The white and gray dashed lines indicate the position and orientation of the gold and aluminum antennas, the gray arrow shows the geometrical shift of the aluminum antennas in the experiment.

In the following, we would like to analyze the behavior of the measured x -polarized SH signals and in particular, the peak in the SH generation intensity that appears at $x_1 \approx 80$ nm. We will see that the radiated SH signals can be described by a SH near-field distribution of a SH dipole that is oriented along the y -direction and located in the center of the gold nanoantennas.

In order to understand and describe the experimental results in the most straightforward way, we utilize a single static electric dipole at 2ω . Despite the simplicity, this model describes the observed behavior of the radiated SH signals very well. The electric field of a static electric dipole is given by⁴⁹

$$\mathbf{E}_{2\omega}^D(\mathbf{r}) = \frac{1}{4\pi\epsilon_0} \left(3 \frac{\mathbf{p}_{2\omega} \cdot \mathbf{r}}{r^5} \mathbf{r} - \frac{1}{r^3} \mathbf{p}_{2\omega} \right) \quad (1)$$

where ϵ_0 is the vacuum permittivity, $\mathbf{p}_{2\omega}$ corresponds to the SH dipole moment located in the gold volume of the nanoantennas,⁵⁰ and \mathbf{r} is the spatial coordinate.

In Figure 3b, we display the x -component of the near-field intensity $I_{2\omega,x}^D \propto (E_{2\omega,x}^D)^2$ for a SH dipole that points toward the y -direction in the plane of the dipole nanoantennas ($z = 0$) derived from eq 1, together with the experimental arrangement

of the gold and the aluminum nanoantennas. The gray arrow indicates the shift of the aluminum antennas. On this path, we start from a field node at $x_1 = 0$ nm, move toward and over a SH field maximum, and reach near zero SH intensity for large offsets x_1 , very similar to the results of the experiment.

Equation 1 also allows to analytically derive an expression for the x -component of the SH near-field intensity $I_{2\omega,x}^D$ where we obtain

$$I_{2\omega,x}^D(x_1, y_1) \propto \frac{x_1^2 y_1^2}{(x_1^2 + y_1^2)^5} p_{2\omega}^2 \quad (2)$$

This expression displays a fit-function for the measured SH intensities. The fitted SH intensity distribution is plotted in Figure 3a together with the measured SH intensities. The free parameters in this fit are the distance in y -direction between the center of the gold and the aluminum nanoantennas y_1 as well as an overall amplitude, corresponding to the magnitude of the SH dipole moment $p_{2\omega}$. Overall, we find good agreement between the experiment and the dipolar model. In particular, the dipole equation describes the peak in the radiated x -polarized SH intensity at an intermediate aluminum antenna offset x_1 of about 80 nm.

It should be stressed that the overall shape of the measurements from Figure 3a cannot be described by a SH dipole oriented along the gold nanoantenna long axis. Furthermore, an additional contribution to the SH response from the aluminum nanoantennas driven by the enhanced near-field of the gold nanoantennas at the fundamental wavelength can also not describe the measurements of Figure 3a. The two just described scenarios would lead to a maximum in the x -component of the SH near-field intensity for $x_1 = 0$ nm, which we do not observe in the experiment and hence they can most likely be excluded as possible explanations.

In the next step, we are going to probe the y -component of the SH near-field distribution of the gold nanoantennas by placing aluminum nanoantennas close to the gold nanoantennas, which are oriented along the y -direction, hence perpendicular to the gold nanoantennas. In particular, we probe the y -component of the SH near-field at $x_2 = 0$ nm, that is, centered with respect to the gold nanoantennas, and at different positions y_2 of the aluminum nanoantennas. Figure 4a illustrates the corresponding experiment, and SEM images of a fabricated nanoantenna array are shown in Figure 4b.

Similar to the experiments above, we shift the aluminum nanoantennas in small steps of nominally 10 nm from a large distance y_2 of about 155 nm to almost contact with $y_2 \approx 75$ nm, which corresponds to a gap distance Δs ranging from 80 to 0 nm; see the inset and the SEM images in Figure 5a. The position of the aluminum antennas has almost no influence on the plasmon resonance of the gold nanoantennas, which can be deduced from simulated near-field distributions and measured linear optical transmittance spectra, which are shown in the Figures S2 and S4, respectively. For the different gap distances g , we measure the y -polarized SH intensity for excitation at 1060 nm, which are also depicted in Figure 5a. Noteworthy, because the antenna arrays studied in Figures 3a and 5a are located on two different samples, the overall SH intensity can vary and therefore a quantitative comparison of the absolute SH signal strength between the two experiments is limited, even though the antennas have been fabricated with nominally equal parameters.

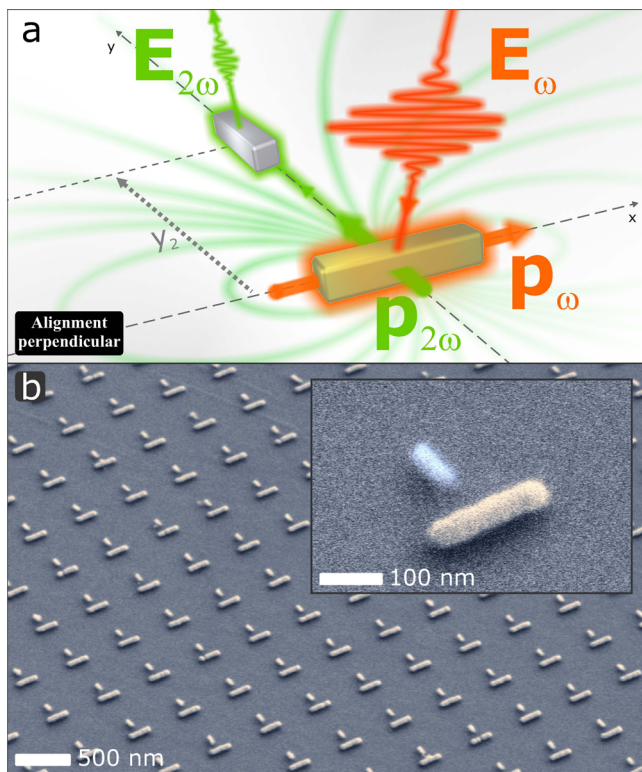


Figure 4. (a) Graphical illustration of the experiment: Probing the y -component of the local SH near-field of gold nanoantennas. (b) Colored-tilted SEMs of a corresponding sample.

We find a large increase of the y -polarized SH signal strength for decreasing gap distance Δs . In order to analyze the observed behavior, we use the model introduced above, however, now we are studying the y - instead of the x -component. The corresponding near-field intensity $I_{2\omega,y}^D$ is shown in Figure 5b. In accordance with the experiment, we find a strong increase in the y -component of the near-field intensity $I_{2\omega,y}^D$ when moving the aluminum antennas toward the center of the gold nanoantennas.

The functional behavior of this increase can be once more derived from the dipole eq 1. For the y -component of the near-field intensity $I_{2\omega,y}^D$ at $x_2 = 0$ nm we obtain

$$I_{2\omega,y}^D(y_2) \propto \frac{1}{y_2^n} p_{2\omega}^2 \quad (3)$$

According to eq 1 the y -component of the near-field intensity $I_{2\omega,y}^D$ increases with decreasing gap distance as $1/y_2^6$. In our analysis, however, we use the exponent n as a free fit parameter in addition to the overall amplitude $p_{2\omega}$. The fit to the y -polarized SH intensities using eq 3 is shown in Figure 5a together with the measured SH signals. The fit delivers $n \sim 5.2$, which is quite close to the expectation. The small difference can be attributed to the simplified model that we used to describe the SH near-field of the gold nanoantennas, which does not take the precise geometrical parameters of the nanoantennas into account. Also, for a very small gap distance Δs of below about 20 nm the gold nanoantennas begin to feel the presence of the aluminum nanoantennas, that is, a change in their dielectric environment. This leads to small variations in the linear optical response of the gold nanoantennas, which also influences their nonlinear optical response,^{51,52} see Figure S4 for the linear optical spectra of the corresponding nanoantenna

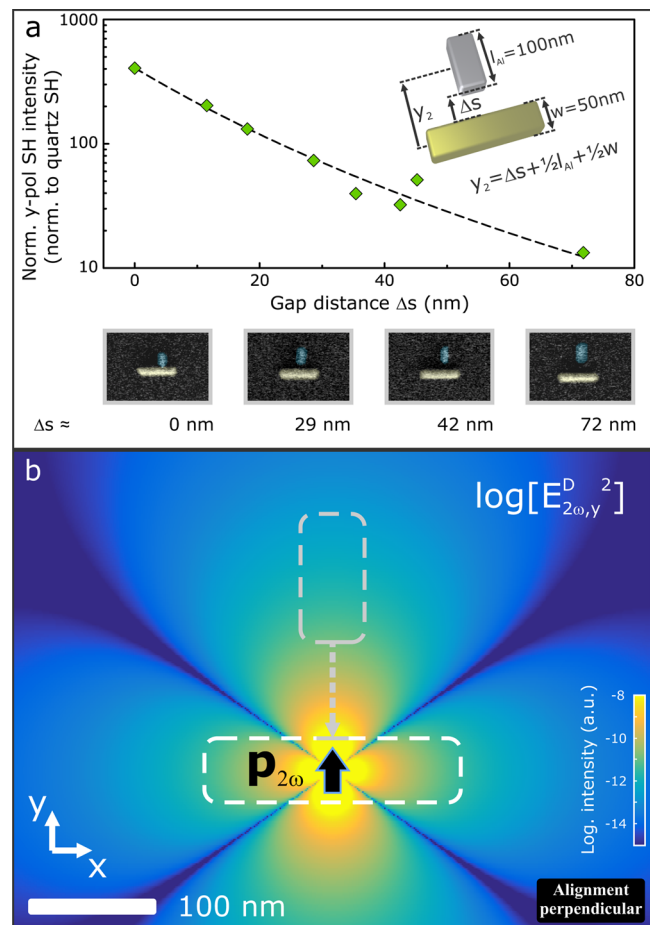


Figure 5. (a) Measured y -polarized SH intensity as a function of the gap distance Δs between the gold and the aluminum nanoantennas. The black dashed line corresponds to a fitted dipolar intensity distribution using eq 3. The insets below show exemplary colored SEM images. (b) Dipole field intensity distributions of the y -component of a static electric SH dipole $p_{2\omega}$ oriented along the y -direction. The white and gray dashed lines indicate the position and orientation of the gold and aluminum antennas and the gray arrow shows the geometrical shift of the aluminum antennas in the experiment.

arrays. However, our simple and straightforward model gives a very intuitive explanation of the general observations from the experiments.

It is important to note that the measured y -polarized SH intensities from Figure 5a can also not be described and modeled by a SH dipole that is aligned parallel to the gold nanoantenna long axis, which would exhibit for all gap distances Δs a field node at $x_2 = 0$ nm.

Recapitulating, the near-field SH measurements strongly indicate that the SH dipole of the gold nanoantennas is predominantly oriented in a perpendicular fashion with respect to the gold nanoantenna long axis, although we excite the nanoantennas with light polarized along the nanoantennas. Here, we would like to briefly discuss a possible reason for the origin of this polarization behavior. There are two important facts that have to be taken into account: First, when measuring linear transmittance spectra of a bare gold nanoantenna array for an incident polarization that is oriented perpendicular to the gold nanoantenna long axis we also find a weak plasmon resonance that is located in our SH wavelength range. This

plasmon resonance can boost the SH emission in the perpendicular polarization direction.^{31,53} Second, the longitudinal plasmon resonance occurs at a wavelength of about 1040 nm. Hence, the generated *x*-polarized SH field at about 520 nm drives the longitudinal plasmon resonance far above its localized plasmon resonance frequency. Therefore, the longitudinal plasmon cannot follow the fast oscillation of the SH field and hence, the emission along the gold nanoantenna long axis is suppressed and diminished by the longitudinal plasmon resonance. These two contributions, the enhanced SH emission supported by the perpendicular plasmon resonance located at the SH wavelength and the suppression of the SH emission by the longitudinal plasmon resonance, can be captured in a simple oscillator model of the nonlinear response⁵³ and can explain the about 2 orders of magnitude difference in the SH signal of the two polarization components.

To summarize, we introduced and demonstrated a novel method that allows probing of the local second-harmonic near-field of plasmonic nanostructures in a polarization-resolved fashion. As a local sensor, this method utilizes oriented and hence polarization sensitive aluminum nanoantennas that are resonant to the second-harmonic field. As an example, in this Letter we presented measurements of the polarization-resolved second-harmonic near-field distribution of gold dipole nanoantennas. In the near-field measurements, we find an intriguing and unexpected polarization behavior of the SH response of the gold nanoantennas. Beyond the measurement of the nonlinear near-field of dipole nanoantennas, this method could also be used to study the nonlinear near-field distribution of more complex plasmonic structures, for example, plasmonic split ring resonators. We believe that our novel method, namely the use of resonant plasmonic nanoantennas as local sensors for the measurement of nonlinear local electric fields, will find widespread implementation and applications in scanning near-field optical microscopies for nonlinear nanoimaging. Furthermore, this work paves the way toward more complex plasmonic elements with engineered nonlinear optical properties for photonic integrated circuitry.

■ ASSOCIATED CONTENT

■ Supporting Information

The Supporting Information is available free of charge on the ACS Publications website at DOI: [10.1021/acs.nanolett.6b05285](https://doi.org/10.1021/acs.nanolett.6b05285).

Figure S1, measured raw spectra of second-harmonic generation from a bare gold and a bare aluminum antenna array. Figure S2, simulated electric near-field distributions of the antenna geometries investigated in the manuscript. Figure S3, measured transmittance spectra of the nanoantenna arrays investigated in Figure 2 and Figure 3. Figure S4, measured transmittance spectra of the nanoantenna arrays investigated in Figure 4 and Figure 5 (PDF)

■ AUTHOR INFORMATION

Corresponding Author

*E-mail: b.metzger@physik.uni-stuttgart.de.

ORCID

Bernd Metzger: 0000-0002-9027-8676

Notes

The authors declare no competing financial interest.

■ ACKNOWLEDGMENTS

We gratefully acknowledge financial support from the Baden-Württemberg Stiftung (Kompetenznetz Funktionelle Nanostrukturen), from the DFG (SPP1391, ultrafast nanooptics), from the BMBF (13N10146), and the ERC (Complexplas).

■ REFERENCES

- (1) Hell, S. W.; Wichmann, J. *Opt. Lett.* **1994**, *19*, 780–782.
- (2) Betzig, E.; Patterson, G. H.; Sougrat, R.; Lindwasser, O. W.; Olenych, S.; Bonifacino, J. S.; Davidson, M. W.; Lippincott-Schwartz, J.; Hess, H. F. *Science* **2006**, *313*, 1642–1645.
- (3) Schmidt, O.; Bauer, M.; Wiemann, C.; Porath, R.; Scharfe, M.; Andreyev, O.; Schönhense, G.; Aeschlimann, M. *Appl. Phys. B: Lasers Opt.* **2002**, *74*, 223–227.
- (4) Novotny, L.; Hecht, B. *Principles of Nano-Optics*; Cambridge University Press, 2006.
- (5) Atkin, J. M.; Sass, P. M.; Teichen, P. E.; Eaves, J. D.; Raschke, M. B. *J. Phys. Chem. Lett.* **2015**, *6*, 4616–4621.
- (6) Jäger, S.; Kern, A. M.; Hentschel, M.; Jäger, R.; Braun, K.; Zhang, D.; Giessen, H.; Meixner, A. J. *Nano Lett.* **2013**, *13*, 3566–3570.
- (7) Neuman, T.; Alonso-González, P.; García-Etxarri, A.; Schnell, M.; Hillenbrand, R.; Aizpurua, J. *Laser and Photonics Reviews* **2015**, *9*, 637–649.
- (8) Liu, N.; Tang, M. L.; Hentschel, M.; Giessen, H.; Alivisatos, A. P. *Nat. Mater.* **2011**, *10*, 631–636.
- (9) Shen, Y.; Zhou, J.; Liu, T.; Tao, Y.; Jiang, R.; Liu, M.; Xiao, G.; Zhu, J.; Zhou, Z.-K.; Wang, X. *Nat. Commun.* **2013**, *4*, x.
- (10) Butet, J.; Martin, O. J. F. *Nanoscale* **2014**, *6*, 15262–15270.
- (11) Neubrech, F.; Pucci, A.; Cornelius, T. W.; Karim, S.; García-Etxarri, A.; Aizpurua, J. *Phys. Rev. Lett.* **2008**, *101*, 157403.
- (12) Adato, R.; Yanik, A. A.; Amsden, J. J.; Kaplan, D. L.; Omenetto, F. G.; Hong, M. K.; Erramilli, S.; Altug, H. *Proc. Natl. Acad. Sci. U. S. A.* **2009**, *106*, 19227–19232.
- (13) Kauranen, M.; Zayats, A. V. *Nat. Photonics* **2012**, *6*, 737–748.
- (14) Hasan, S. B.; Lederer, F.; Rockstuhl, C. *Mater. Today* **2014**, *17*, 478–485.
- (15) Suh, J. Y.; Odom, T. W. *Nano Today* **2013**, *8*, 469–479.
- (16) Tame, M. S.; McEnery, K. R.; Ozdemir, S. K.; Lee, J.; Maier, S. A.; Kim, M. S. *Nat. Phys.* **2013**, *9*, 329–340.
- (17) Olmon, R. L.; Rang, M.; Krenz, P. M.; Lail, B. A.; Saraf, L. V.; Boreman, G. D.; Raschke, M. B. *Phys. Rev. Lett.* **2010**, *105*, 167403.
- (18) Zavelani-Rossi, M.; Celebrano, M.; Biagioni, P.; Polli, D.; Finazzi, M.; Duó, L.; Cerullo, G.; Labardi, M.; Allegrini, M.; Grand, J.; et al. *Appl. Phys. Lett.* **2008**, *92*, 093119.
- (19) Zhang, Y.; Grady, N. K.; Ayala-Orozco, C.; Halas, N. J. *Nano Lett.* **2011**, *11*, 5519.
- (20) Hanke, T.; Cesar, J.; Knittel, V.; Trügler, A.; Hohenester, U.; Leitenstorfer, A.; Bratschitsch, R. *Nano Lett.* **2012**, *12*, 992–996.
- (21) Aouani, H.; Navarro-Cia, M.; Rahmani, M.; Sidiropoulos, T. P. H.; Hong, M.; Oulton, R. F.; Maier, S. A. *Nano Lett.* **2012**, *12*, 4997–5002.
- (22) Hentschel, M.; Utikal, T.; Giessen, H.; Lippitz, M. *Nano Lett.* **2012**, *12*, 3778–3782.
- (23) Linden, S.; Niesler, F. B. P.; Förstner, J.; Grynko, Y.; Meier, T.; Wegener, M. *Phys. Rev. Lett.* **2012**, *109*, 1.
- (24) Harutyunyan, H.; Volpe, G.; Quidant, R.; Novotny, L. *Phys. Rev. Lett.* **2012**, *108*, 217403.
- (25) Thyagarajan, K.; Rivier, S.; Lovera, A.; Martin, O. J. F. *Opt. Express* **2012**, *20*, 12860–12865.
- (26) Czaplicki, R.; Husu, H.; Siikaniemi, R.; Mäkitalo, J.; Kauranen, M.; Laukkanen, J.; Lehtolahti, J.; Kuittinen, M. *Phys. Rev. Lett.* **2013**, *110*, 093902.
- (27) Zhang, Y.; Wen, F.; Zhen, Y.-R.; Nordlander, P.; Halas, N. J. *Proc. Natl. Acad. Sci. U. S. A.* **2013**, *110*, 9215–9219.
- (28) Lee, J.; Tymchenko, M.; Argyropoulos, C.; Chen, P. Y.; Lu, F.; Demmerle, F.; Boehm, G.; Amann, M. C.; Alu, A.; Belkin, M. A. *Nature* **2014**, *511*, 65–69.

- (29) Valev, V. K.; Baumberg, J. J.; De Clercq, B.; Braz, N.; Zheng, X.; Osley, E. J.; Vandendriessche, S.; Hojeij, M.; Blejean, C.; Mertens, J.; et al. *Adv. Mater.* **2014**, *26*, 4074–4081.
- (30) Viarbitskaya, S.; Demichel, O.; Cluzel, B.; Colas des Francs, G.; Bouhelier, A. *Phys. Rev. Lett.* **2015**, *115*, 197401.
- (31) Linnenbank, H.; Linden, S. *Optica* **2015**, *2*, 698–701.
- (32) Celebrano, M.; Wu, X.; Baselli, M.; Grossmann, S.; Biagioni, P.; Locatelli, A.; De Angelis, C.; Cerullo, G.; Osellame, R.; Hecht, B.; et al. *Nat. Nanotechnol.* **2015**, *10*, 412–417.
- (33) O'Brien, K.; Suchowski, H.; Rho, J.; Salandrino, A.; Kante, B.; Yin, X.; Zhang, X. *Nat. Mater.* **2015**, *14*, 379–383.
- (34) Li, G.; Chen, S.; Pholchai, N.; Reineke, B.; Wong, P. W. H.; Pun, E. Y. B.; Cheah, K. W.; Zentgraf, T.; Zhang, S. *Nat. Mater.* **2015**, *14*, 607–612.
- (35) Lee, J.; Nookala, N.; Gomez-Diaz, J. S.; Tymchenko, M.; Demmerle, F.; Boehm, G.; Amann, M.-C.; Alú, A.; Belkin, M. A. *Adv. Opt. Mater.* **2016**, *4*, 664–670.
- (36) Knight, M. W.; Liu, L.; Wang, Y.; Brown, L.; Mukherjee, S.; King, N. S.; Everitt, H. O.; Nordlander, P.; Halas, N. J. *Nano Lett.* **2012**, *12*, 6000–6004.
- (37) Knight, M. W.; King, N. S.; Liu, L.; Everitt, H. O.; Nordlander, P.; Halas, N. J. *ACS Nano* **2014**, *8*, 834–840.
- (38) Gucciardi, P. G.; Bachelier, G.; Allegrini, M. *J. Appl. Phys.* **2006**, *99*, 124309.
- (39) Höppener, C.; Beams, R.; Novotny, L. *Nano Lett.* **2009**, *9*, 903–908.
- (40) Dregely, D.; Neubrech, F.; Duan, H.; Vogelgesang, R.; Giessen, H. *Nat. Commun.* **2013**, *4*, 2237.
- (41) Niesler, F. B. P.; Feth, N.; Linden, S.; Wegener, M. *Opt. Lett.* **2011**, *36*, 1533–1535.
- (42) Metzger, B.; Gui, L.; Giessen, H. *Opt. Lett.* **2014**, *39*, 5293–5296.
- (43) Metzger, B.; Hentschel, M.; Lippitz, M.; Giessen, H. *Opt. Lett.* **2012**, *37*, 4741–4743.
- (44) Boyd, R. W. *Nonlinear Optics*, 3rd ed.; Academic Press, Elsevier, 2008.
- (45) Birss, R. R. *Symmetry and Magnetism*; North-Holland Publishing Co.: Amsterdam, 1966.
- (46) Canfield, B. K.; Husu, H.; Laukkanen, J.; Bai, B.; Kuittinen, M.; Turunen, J.; Kauranen, M. *Nano Lett.* **2007**, *7*, 1251–1255.
- (47) Butet, J.; Thyagarajan, K.; Martin, O. J. F. *Nano Lett.* **2013**, *13*, 1787–1792.
- (48) Kreibig, U.; Vollmer, M. *Optical Properties of Metal Clusters*; Springer-Verlag: Berlin Heidelberg, 1995; p 69–72.
- (49) Jackson, J. D. *Classical Electrodynamics*, 3rd ed.; Wiley: New York, 1998.
- (50) Wolf, D.; Schumacher, T.; Lippitz, M. *Nat. Commun.* **2016**, *7*, 10361.
- (51) Metzger, B.; Hentschel, M.; Schumacher, T.; Lippitz, M.; Ye, X.; Murray, C. B.; Knabe, B.; Buse, K.; Giessen, H. *Nano Lett.* **2014**, *14*, 2867–2872.
- (52) Linnenbank, H.; Grynko, Y.; Foerstner, J.; Linden, S. *Light: Sci. Appl.* **2016**, *5*, e16013.
- (53) Metzger, B.; Gui, L.; Fuchs, J.; Floess, D.; Hentschel, M.; Giessen, H. *Nano Lett.* **2015**, *15*, 3917–3922.